Journal of Computational Physics **160,** 564–576 (2000)
doi:10.1006/jcph.2000.6473, available online at http://www.idealibrary.com on IDEAL®

Low-Dimensional Approximations of Multiscale Epitaxial Growth Models for Microstructure Control of Materials

S. Raimondeau* and D. G. Vlachos†

Department of Chemical Engineering, University of Massachusetts, Amherst, Massachusetts 01003-3110
E-mail: *sraimond@athina.ecs.umass.edu, †vlachos@risky.ecs.umass.edu

Received September 28, 1999; revised February 10, 2000

The desire to control the microstructure of materials during growth has recently led to the development of multiscale models combining molecular information from microscopic scales with continuum-type information at macroscopic scales. Such multiscale models for epitaxial growth are here reduced through proper orthogonal decomposition to obtain low-dimensional approximations that can be useful for on-line control. The approach is illustrated in a stagnation flow microreactor by examining the effects of substrate temperature and inlet composition on film morphology. Numerically, this is the first attempt to describe the dynamics of coupled deterministic partial differential equations and stochastic partial differential equations (a master equation) with a small set of ordinary differential equations. Reduction is carried for both the fluid phase and the film morphology at different operating conditions. It is found that while information generated by molecular models can be represented by relatively low-dimensional deterministic models, the minimum necessary reduced model dimension for description of microscale features of epitaxial films is higher than that needed for fluid phase species concentrations. Trained models obtained from model reduction can be used for nearby parameter changes.

INTRODUCTION

The desire to control the microstructure of nanophase materials and thin films at the molecular level is a well-established trend and underscores the need for fundamental mathematical models describing crystal growth interacting with the surrounding fluid. A major challenge in developing such models is that epitaxial growth of materials is a typical example where multiple time and length scales are encountered, as shown schematically in the inset of Fig. 1. For microscopic scales on the one hand, molecular models such as Monte Carlo (MC) and molecular dynamics simulations are required to properly capture the spatiotemporal evolution of pattern formation including nucleation, cluster–cluster

0021-9991/00 $35.00

coalescence, adsorbate-adsorbate interactions, and impurities. For macroscopic scales, on the other hand, continuum-type partial differential equations (PDEs) are typically used to describe the conservation equations of continuity, momentum, energy, and species.

The disparity in scales of these processes and the computational demand of molecular models renders direct modeling of an entire reactor using a molecular model intractable. To overcome this difficulty, multiscale integration hybrid (MIH) algorithms have recently been introduced to model catalytic reactors [1], epitaxial growth [2], chemical vapor deposition [3], and flow through tubes [4]. The basic idea of MIH algorithms is to decompose the domain into two subdomains, one for the macroscopic scale (fluid phase) and one for the microscopic scale (top layers of the film in our case). The PDEs characterizing the fluid phase are then discretized and solved through a conventional method, such as a finite difference scheme and Newton's algorithm for steady-state or the method of lines for time-dependent situations. The surface is modeled with a master equation (a stochastic partial differential equation or SPDE) that is solved using a continuous time MC algorithm [5]. The coupling of the two subdomains is done at the fluid–film interface through a homogenization of the boundary conditions, i.e., incorporation of mesoscopically average rates computed from the molecular model into the boundary conditions of the fluid phase model.

Despite demonstration of the feasibility of such MIH algorithms, such direct numerical simulations (DNS) are very demanding, making use of MIH algorithms an impractical tool for on-line control of microstructure of materials. Since the governing coupled deterministic PDEs and stochastic master equations are infinite dimensional systems, a successful method to describe them by a low-dimensional system of ordinary differential equations represents an important step for on-line control of microstructure of materials, based on fundamental models. Here, we demonstrate application of the proper orthogonal decomposition (POD) technique or Karhunen–Loeve expansion to multiscale models in order to meet this objective.

MULTISCALE MODEL

To illustrate the approach, a stagnation-point flow reactor is chosen to model the deposition of a precursor transferred with a carrier gas (hydrogen in our case) on a hot substrate at atmospheric pressure (see inset in Fig. 1). The precursor is transported from the bulk of the fluid to the surface by convection and diffusion and no gas-phase chemistry is considered. A similarity transformation converts the two-dimensional fluid mechanics, continuity, heat, and mass transfer conservation equations into a one-dimensional problem. The transformed equations are [6]

$$\frac{\partial}{\partial \tau}\left(\frac{\partial f}{\partial \eta}\right) = \frac{\partial^3 f}{\partial \eta^3} + f\frac{\partial^2 f}{\partial \eta^2} + \frac{1}{2}\left(\frac{\rho_b}{\rho} - \left(\frac{\partial f}{\partial \eta}\right)^2\right) \tag{1}$$

$$\frac{\partial T}{\partial \tau} = \frac{1}{\mathrm{Pr}}\frac{\partial^2 T}{\partial \eta^2} + f\frac{\partial T}{\partial \eta} \tag{2}$$

$$\frac{\partial y_j}{\partial \tau} = \frac{1}{\mathrm{Sc}_j}\frac{\partial^2 y_j}{\partial \eta^2} + f\frac{\partial y_j}{\partial \eta}, \tag{3}$$

where f is the stream function, τ is the dimensionless time, η is the dimensionless distance to the surface, ρ is the density of the mixture, ρ_b is the density of the mixture in the bulk,

T is the temperature, Pr is the Prandtl number, y_j is the mole fraction of species j in the gas mixture, and Sc_j is the Schmidt number of species j. The Prandtl number is assumed to be constant and the Schmidt number is species dependent, as indicated in Eq. (3).

The boundary conditions for the macroscopic problem are given by the following equations, assuming no slip and slow growth at the surface:

$$\text{Bulk } T = T_\mathrm{b}, \qquad \frac{\partial f}{\partial \eta} = 1, \qquad y_j = y_{j\mathrm{b}} \tag{4–6}$$

$$\text{Surface } f = 0, \qquad \frac{\partial f}{\partial \eta} = 0, \qquad T = T_\mathrm{s}. \tag{7–9}$$

Furthermore, the surface is inert for the species not participating in the growth:

$$\frac{\partial y_j}{\partial \eta} = 0 \qquad \text{for } j \neq \text{growing} \tag{10}$$

$$\frac{\partial y_{\text{growing}}}{\partial \eta} = \frac{M_j}{M}\mathrm{Sc}_j(r'_\mathrm{a} - r'_\mathrm{d}), \qquad \text{for adsorbing species;} \tag{11}$$

here M_j is the molecular weight of species j, M is the average molecular weight, and r'_a and r'_d are the dimensionless rate of adsorption and desorption, respectively. The adsorption and desorption rates are computed as spatial averages from the MC simulation at each time step [2].

Due to high dilution, the mass transfer problem can be decoupled from the fluid–heat transfer one and solved separately. The conservation equations are discretized using a finite difference scheme on 101 nodes. Newton's method is used for the steady-state solution of the flow–heat problem, and the method of lines for the time-dependent mass transfer problem where transients are considered [7].

Once the precursor arrives at the surface, it participates in microscopic phenomena, including adsorption, desorption, and migration on the surface. Only first-nearest-neighbor interactions with bond energy of 17 kcal/mol and the solid-on-solid approximation of a simple cubic lattice are considered for demonstration of the approach. The adsorption transition probability is computed from the kinetic theory of gases with a sticking coefficient of 0.1. Desorption and surface migration follow Arrhenius kinetics and depend on the local microenvironment of each adsorbed atom (for details of the probabilities and coupling issues see [2]).

The surface changes in time and space are described according to the master equation

$$\frac{dP_\alpha}{dt} = \sum_\beta [W_{\alpha\beta}P_\beta - W_{\beta\alpha}P_\alpha], \tag{12}$$

where P_α is the probability of the surface being in configuration α and $W_{\alpha\beta}$ is the transition probability per unit time of the surface going from configuration β to α. Since such a SPDE cannot generally be solved analytically, MC methods are often employed. Using a continuous time MC algorithm with classes of microscopic processes and local update of the transition probabilities and surface configuration, efficient simulations are carried out so that sufficiently long times are reached [2]. A lattice size of 120×120 is used for simulating a (40, 1, 0) misoriented surface.

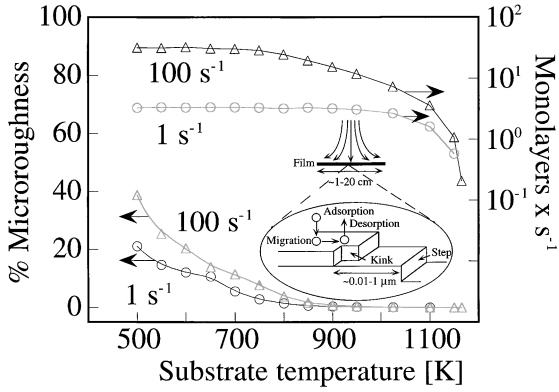

FIG. 1. Relative film microroughness over a perfect surface and corresponding growth rate in monolayers/s versus the surface temperature for two strain rates indicated. A transition from step flow mode to two-dimensional nucleation with a concomitant increase in growth rate is found as the substrate temperature decreases. The points are simulation data and the lines just connect them. The inset shows a schematic of the stagnation flow reactor depicting the different length scales involved.

Figure 1 shows the relative film microroughness and the corresponding growth rates versus the surface temperature for two strain rates (velocity gradient outside the boundary layer) indicated, in the limit of no surface diffusion (qualitatively similar behavior is found in the presence of surface diffusion [2]). The microroughness, representing the number of broken bonds, is defined as

$$1 + \frac{\sum_{i,j=1}^{N_s} (|h_{i+1,j} - h_{i,j}| + |h_{i-1,j} - h_{i,j}| + |h_{i,j+1} - h_{i,j}| + |h_{i,j-1} - h_{i,j}|)}{2 \times N_s \times N_s}, \quad (13)$$

where $N_s \times N_s$ is the lattice size, and $h_{i,j}$ is the height of site i, j on the surface. Using Eq. (13), the relative, compared to the perfect (no defects) misoriented surface, film microroughness is then plotted in all figures. Different growth modes are observed, namely step flow at high temperatures and two-dimensional nucleation at low temperatures. At high temperatures, molecules have sufficient time to reach favorable positions on the surface (kinks and steps) due to fast desorption followed by readsorption. The corresponding growth rate is low because of the fast-activated desorption rate that establishes a partial equilibrium near the gas–solid interface. At sufficiently lower temperatures, on the other hand, an increase in growth rate is observed in Fig. 1 caused by slow desorption that leads to a high supersaturation of adatoms between steps, favoring the two-dimensional nucleation growth mode. According to Fig. 1, two temperatures (600 and 1100 K), representative of the two different growth modes, were chosen for model reduction by POD described next.

PROPER ORTHOGONAL DECOMPOSITION

The POD was first used in meteorology under the name of "method of empirical orthogonal eigenfunctions" by Lorenz [8] and was further developed by Lumley [9] for identification of coherent structures in fluid mechanics. The POD is used to reduce temporal or spatiotemporal data of complex dynamic models to low-dimensional systems. The

purpose of the POD decomposition is to extract an optimal basis of eigenfunctions describing the low dimensionality of the problem while capturing the proper dynamics. These eigenfunctions are obtained from the diagonalization of the two-point correlation matrix (Karhunen–Loeve expansion theorem) from a given set of numerical or experimental data [10]. Sirovich [11] demonstrated that using a time correlation matrix, instead, yielded the same low-dimensional system while reducing significantly the size of the correlation matrix, especially for two-dimensional problems, making eigenvalue analysis a tractable computation. For reduction of systems of partial differential equations, the Galerkin method may then be used to obtain the final linear model. The Galerkin method is used to extract the time-dependent coefficients of the final linear reduced model using the underlying PDEs of the given problem. This is done by optimizing the error between the "exact" solution, obtained through direct numerical integration of the original PDEs, and the truncated linear approximation. When reducing experimental results, the Galerkin approach cannot be used, so instead, the data are projected onto the basis of eigenfunctions to give the desired reduction.

The POD has already been applied to different experimental and model systems. Many examples of this method can be found in the study of turbulent flows [11–15]. Aside from fluid flow problems, other examples include the catalytic CO oxidation on a Pt crystal surface [16], macroinstabilities in the velocity data of a cylindrical stirred tank [17], nonlinear reaction–diffusion problems [18] for control purposes, and nonlinear model reduction of rapid thermal processing [19], to name a few. It has been shown that the Karhunen–Loeve–Galerkin procedure (another name for the POD reduction applied to a set of PDEs) is successful even when other conventional orthonormal sets of eigenfunctions, e.g., polynomials or trigonometric, fail to provide low-dimensional approximation in a complex geometry [20]. Compared to other existing reduction methods, such as the computational singular perturbation and low-dimensional manifold theory [21, 22], the POD technique is attractive, as it can deal with both equations (through Galerkin's procedure) and experimental data, treating them as snapshots. This is particularly important here, as we have no close form equations for the surface.

The underlying mathematics is described by Berkooz *et al.* [13]. The following outlines the algorithm used based on the method of snapshots. Briefly, let $\{u^{(k)}: k = 1, \ldots, M\}$ be a set of M original snapshots obtained through MIH simulations. The average snapshot $\bar{u} = \frac{1}{M}\sum_{k=1}^{M} u^{(k)}$ is then computed and subtracted from the original data to give a new set $\{v^{(k)}: k = 1, \ldots, M\}$

$$v^{(k)} = u^{(k)} - \bar{u}. \tag{14}$$

The time correlation matrix is defined as

$$(C)_{i,j} = \frac{1}{M}\int_D v^{(i)}(x)v^{(j)}(x)\,dx, \qquad i, j = 1, \ldots, M. \tag{15}$$

The eigenvectors $A^{(n)}$ and the corresponding eigenvalues λ_n of this matrix, needed for the determination of the eigenfunctions Φ_n, are

$$CA^{(n)} = \lambda_n A^{(n)}, \qquad n = 1, \ldots, M \tag{16}$$

and

$$\Phi_n(x) = \sum_{k=1}^{M} A_k^{(n)} v^{(k)}(x), \qquad n = 1, \ldots, M. \tag{17}$$

The truncated series expansion then gives the desired low-dimensional approximation

$$\hat{v}(x,t) = \sum_{n=1}^{N} a_n(t)\Phi_n(x) \tag{18}$$

$$\hat{u}(x,t) = \hat{v}(x,t) + \bar{u}(x), \tag{19}$$

where $a_n(t)$ are the time-dependent coefficients and N represents the number of modes that captures the essence of our problem. This number depends on the eigenvalues, which represent the energy of the system studied. As a first approximation, N should be such that at least 90% of the total energy is captured, and all the other eigenvalues should not be more than 1% of the first eigenvalue [23].

RESULTS AND DISCUSSION

Using the MIH simulations, the particular situation modeled here is related to changes in the bulk mole fraction of the precursor. Such changes are of interest due to perturbations in the inflow composition, startup/shutdown operations, and periodic switching of reactants in heteroepitaxial growth. In particular, after quasi-steady state has been established, the bulk mole fraction of the precursor undergoes a step change, resulting in a dynamic change of the gas-phase concentrations and film morphology. The one-dimensional gas-phase mole fraction data and the quasi-two-dimensional (based on the solid-on-solid approximation) surface configurations are then reduced independently using the POD method. Since there is no close form PDE to describe the stochastic evolution of the surface, as compared to the mass transfer in the fluid phase, snapshots from both phases are treated as experimental configurations. The time-dependent coefficients are computed by projection of these data on the basis set of eigenfunctions.

Gas-Phase Data Reduction

We start first with the reduction of the fluid phase data. Figure 2a shows the time evolution of the gas-phase mole fraction from DNS (solid lines) as well as the POD reduction of the system (dashed lines) at different spatial positions of the boundary layer indicated for conditions corresponding to step flow growth mode. The number of monolayers deposited versus time is also depicted. The growth problem is a fully time dependent one, involving a moving interface (a Stefan problem). However, for relatively low growth rates, after an initial transient, the system attains a quasi-steady state prior to the step change in the precursor's bulk mole fraction; that is, the growth rate, gas-phase mole fractions, and the surface roughness are constant. After the step change indicated by a vertical arrow, at such a low strain rate ($1\,s^{-1}$), a new quasi-steady state is established in a few seconds (or a few monolayers). The reduced model captures very well the dynamic change in the mole fraction at all positions with only 5 modes using 100 snapshots for the reduction. Figure 2b depicts the temporal evolution of the gaseous mole fraction profile from the full simulation

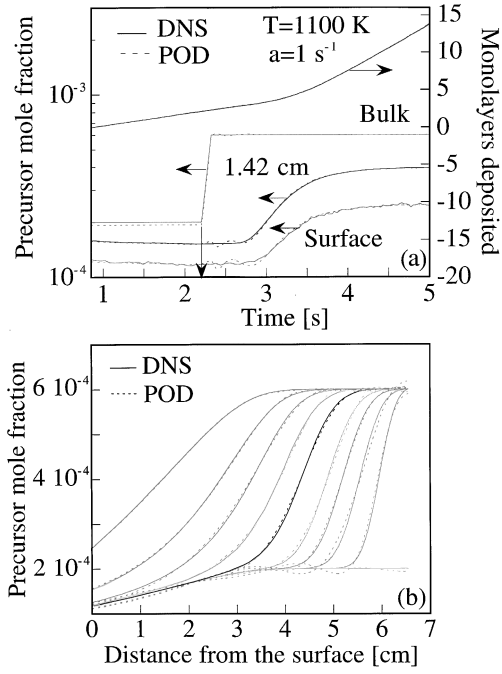

FIG. 2. Time evolution of the precursor mole fraction at three different spatial positions indicated (a) and spatial evolution at times (from right to left) of 2.20, 2.26, 2.32, 2.38, 2.44, 2.56, 2.68, 2.85, 3.12, and 5 s (b) from the direct numerical simulation (solid lines) and the reduced model (dashed lines) with five modes at 1100 K and a strain rate of 1 s^{-1}. Good agreement is found. Panel (a) also shows the number of monolayers deposited versus time. The vertical arrow indicates the instant at which the step change in the precursor's bulk mole fraction occurs.

(solid lines) and the reduced model (dashed lines). Quite good agreement is again seen, except for short times after the step change in the inlet composition near the bulk of the boundary layer, which can further be improved by increasing the number of modes of the reduced model.

It is observed that although the mole fraction of the gaseous species just above the surface has a noisy signal due to the coupling between the deterministic and stochastic models, the POD reduction tends to smooth this signal before and after the step change. Furthermore, as the number of modes in the POD reduction increases, the noise in the mole fraction at the first node (just above the surface) rises. This is, however, undesirable if this model is to be used, in conjunction with measurements of species concentrations near the surface, for on-line control. This noise is caused by the stochastic nature of the MC algorithm and can be reduced only at the expense of a larger lattice in MC simulations. In general, due to the dissipative structure of the mass transfer PDE, noise is diminished very quickly with increasing distance from the surface, resulting in model reduction reminiscent of a purely deterministic model. Overall, it appears that the noise level in MIH simulations is relatively low to allow for model reduction without requiring extraordinary large molecular simulation boxes.

The second and the third columns of Table I give the dominant eigenvalues along with the captured energy as the number of modes increases. Although 99.6% of the energy is captured by the first mode, using just one mode is not enough to reproduce the qualitative shape of the dynamic response of the system. To further illustrate the effect of the number of modes on the spatiotemporal behavior, the relative error (based on the L_2 norm) of the reduced

TABLE I

Eigenvalues, Energy Captured, and Corresponding Deviation of the POD Reduced Model from the Direct Numerical Simulation Solution versus the Number of Modes for Reduction of Gas-Phase Transport Data at 1100 K and 1 s^{-1}

Mode	Eigenvalue	Energy	Modes	% Error
1	9.95×10^{-1}	0.99566931	1	27.80
2	4.14×10^{-3}	0.99981223	5	2.91
3	1.74×10^{-4}	0.99998617	7	1.94
4	1.24×10^{-5}	0.99999853	8	1.90
5	1.20×10^{-5}	0.99999973	9	1.97
6	2.49×10^{-7}	0.99999998	10	2.00
7	1.80×10^{-8}	1.00000000	15	2.29

model $\hat{u}$ compared to the MIH solution u was computed. Results are shown in the last column of Table I. Even though there is an optimal number of modes to obtain the smallest error, the error is only slightly dependent on the number of modes when more than about five modes are kept. The number of modes chosen for the reduction is then based on this error, the total energy captured, as well as a qualitative comparison of the dynamic behavior with the DNS results.

Figures 3a and 3b show the first three spatial eigenfunctions $\Phi_n(x)$ and the time-dependent coefficients $a_n(t)$ of the POD reduction, respectively. The first eigenfunction can

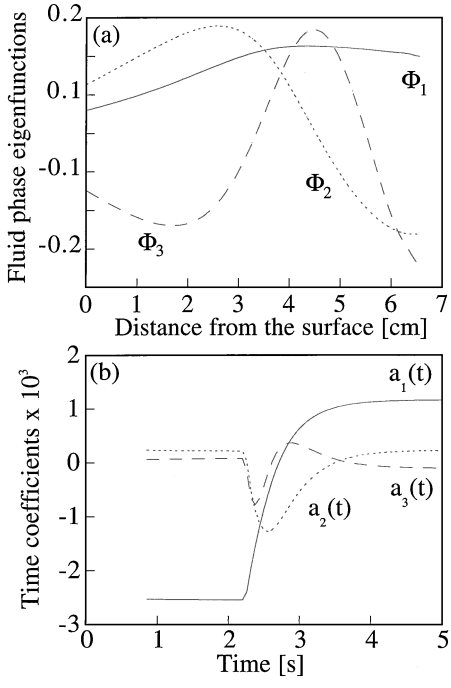

FIG. 3. The first three eigenfunctions (a) and time-dependent coefficients (b) for the fluid-phase reduction shown in Fig. 2. The shape of the first eigenfunction and the corresponding first time dependent coefficient resemble the spatial and temporal evolution of the precursor's mole fraction.

be associated with the general shape of the spatial gaseous mole fraction profile shown in Fig. 2b. The other eigenfunctions appear to be harmonic-like and capture the slight difference in shape at short times following the change in the concentration of the precursor. As for the $a_n(t)$, the first one clearly reflects the time-dependent shape of the response, and the others take into account the noise of the mole fraction. Similar reduction features have been found at other temperatures as well.

Film Morphology Data Reduction

The morphology of the film is one of the most important optimization features in crystal growth, and thus capturing the film microroughness by a reduced model is of interest for on-line control of the entire process. This model reduction situation differs due to the stochastic nature of data generated by MC simulations and proves to be more challenging than the low-noise one-dimensional fluid phase data. To our knowledge, this is the first time that information generated by a molecular simulation has been represented by a small set of ODEs. We have recently shown that similar SPDEs capturing coupled microscopic processes, such as adsorption, desorption, and surface diffusion, can give at sufficiently large length and time scales a mesoscopic (or local mean field) integrodifferential PDE [24]. Under certain conditions, the latter is reminiscent of the classic diffusion–reaction equation (or the Cahn–Hilliard equation), which is known to be dissipative.

Table II depicts the dominant eigenvalues along with the energy captured with increasing number of modes. In fact, with just one mode, while most of the energy is captured ($>$99.99%), only the average morphology (film orientation) of the film is captured without microscopic scale features. It appears that the stochastic nature of a limited number of MC snapshots analyzed by the POD makes identification of coherent structures difficult, so a larger number of modes is required to reasonably reproduce the original pattern. This observation is further rationalized by the fact that most of the remaining eigenvalues are of the same order of magnitude, implying that many modes have a small and similar contribution to the overall film morphology. Choosing an optimal number of modes for the surface reduction is thus more difficult depending on which property one wishes to study. Indeed, while the average height of each snapshot is captured with only one mode, reproducing the microroughness requires a higher-order reduction, as discussed below. More research is needed to exploit whether this is a general feature of molecular simulations.

TABLE II

Eigenvalues, Energy Captured, and Corresponding Deviation of the POD Reduced Model from the Direct Numerical Simulation Solution versus the Number of Modes for Reduction of Film Topology Data at 1100 K and 1 s^{-1}

Mode	Eigenvalue	Energy	Modes	% Error
1	9.99×10^{-1}	0.9999917	1	0.84
2	3.52×10^{-6}	0.9999953	5	0.56
3	3.09×10^{-6}	0.9999983	9	0.53
4	4.83×10^{-7}	0.9999988	10	0.52
5	4.28×10^{-7}	0.9999993	11	0.54
6	2.05×10^{-7}	0.9999995	15	0.56
7	1.75×10^{-7}	0.9999996	25	0.88

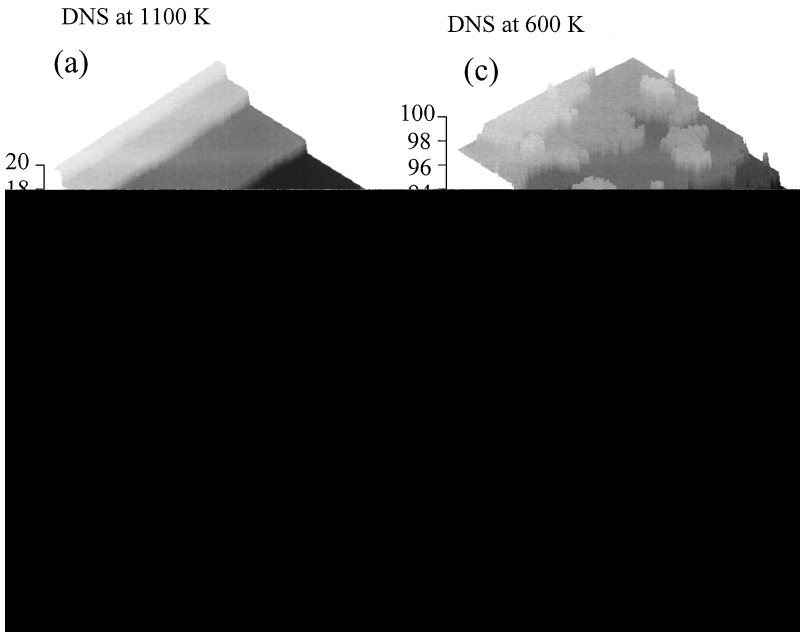

FIG. 4. Snapshots of the film topography from DNS (a) and POD (b) at 1100 K and a strain rate of 1 s^{-1} corresponding to Fig. 2. Panels (c) and (d) show the corresponding snapshots for another reduction at 600 K and a strain rate of 100 s^{-1}. At high temperatures, smooth terraces with fluctuations along the steps are observed. At low temperatures, the topography of the surface is rougher due to two-dimensional nucleation.

As an example, Fig. 4 shows snapshots of the surface morphology from DNS and the POD reduction at $t = 2.7$ s for two different temperatures indicated. At high temperatures (e.g., 1100 K), the surface is smooth (as seen in Fig. 1), and a step change in the precursor's mole fraction has little influence on the growth rate and surface roughness, making experimental sensing of such a change difficult. The morphology of the film predicted with the reduced model using 10 modes, suggested by the minimum error shown in Table II, shows a smoother variation of height compared to the distinct steps of one snapshot of DNS. At lower temperatures (e.g., 600 K) and higher strain rates (e.g., 100 s^{-1}), on the other hand, the surface is microrough and the process is mass transfer limited, so a step change in the precursor's mole fraction leads to a more noticeable increase in the surface microroughness and growth rate. As seen in Fig. 4d, the surface obtained with the reduced model captures the same morphological trends as the one from the DNS for this set of conditions with 20 modes out of 278 snapshots.

Figure 5 shows the first three normalized spatial eigenfunctions Φ_n and the time-dependent coefficients $a_n(t)$. The first eigenfunction is practically flat, explaining the fact that one mode only captures the average morphology contained in the mean (see algorithm above). The rest of the eigenfunctions are oscillatory, giving rise to microscale features. The first time-dependent coefficient clearly has the same shape as the curve representing the number of deposited monolayers versus time (Fig. 2a), which can be associated with the growth rate of the film. The amplitude of the remaining time-dependent coefficients is small.

Next we examine the ability of the POD reduction to capture the film microroughness (a spatially average quantity). Figure 6 shows the microroughness of the surface obtained from the DNS (solid line) and the one reconstructed from the POD reduction

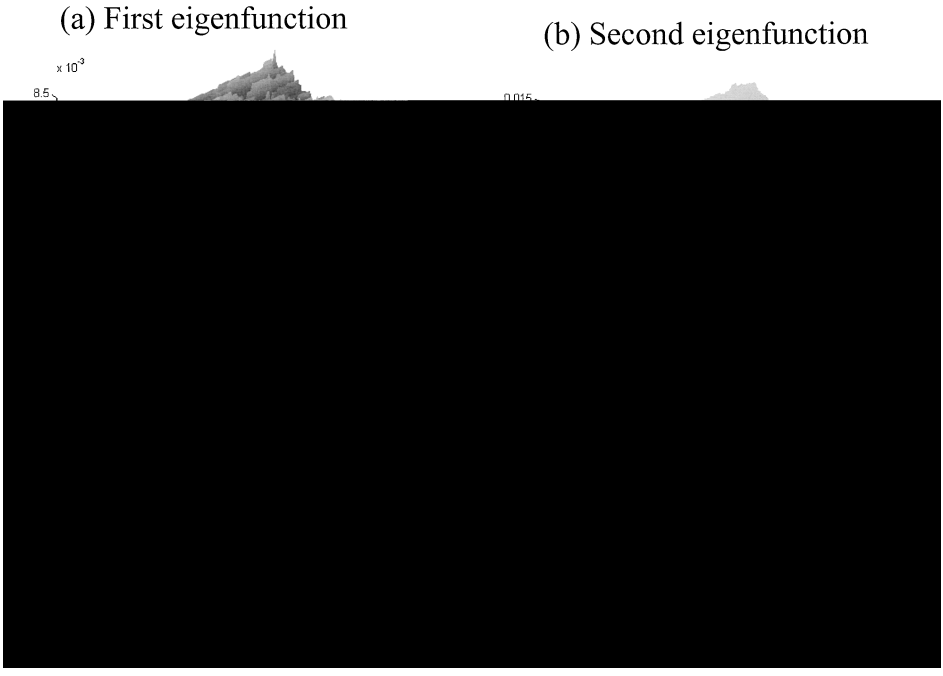

FIG. 5. First three spatial eigenfunctions (a–c) and corresponding time-dependent coefficients (d) for the surface reduction at a temperature of 1100 K and a strain rate of $1\,s^{-1}$ corresponding to Fig. 2. The dominant eigenfunction has a flat shape compared to the remaining eigenfunctions, which are oscillatory.

(dashed line) with 20 modes at 600 K and a strain rate of $100\,s^{-1}$ (see corresponding snapshots in Figs. 4c and 4d). The reduced model is able to reasonably capture the change in the surface microroughness as the precursor's mole fraction changes; better agreement can be achieved by increasing the number of modes. Since microroughness is computed using integers (original snapshots from MC simulations) and real numbers (POD data), respectively, the surface map computed through POD does not exhibit as sharp patterns.

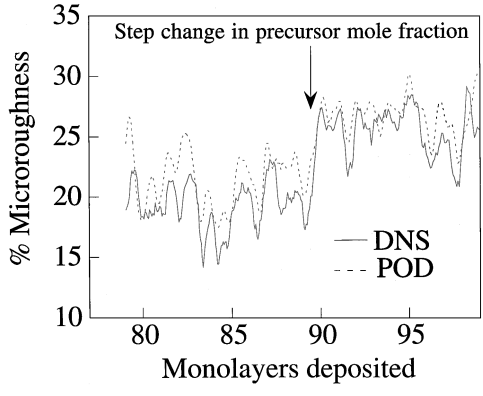

FIG. 6. Film microroughness from the direct numerical simulation (solid lines) and the POD reduction (dashed lines) using 20 modes from 278 snapshots as a function of time at 600 K and a strain rate of $100\,s^{-1}$. The vertical arrow indicates the instant of the step change in the precursor's inlet mole fraction.

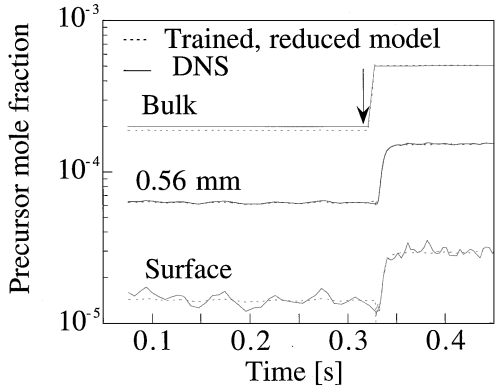

FIG. 7. Predictions of a trained reduced model (dashed lines) for a step change in the precursor's inlet mole fraction from 2×10^{-4} to 5×10^{-4} at three spatial positions indicated along with the corresponding DNS (solid lines) at 600 K and 100 s^{-1}. The vertical arrow indicates the instant of the step change in the precursor's inlet mole fraction.

Toward Use of Reduced Models for Experiments

From a practical point of view, one would be interested in using such a low-dimensional model obtained from first principles' models in conjunction with *in situ* diagnostic techniques for on-line control. To achieve this computationally, a reduced model can be derived at several distinct parameter values representing the desired regime of operation, as has been done with fluid mechanics problems [11, 25]. The derived low-dimensional model can then be used with interpolation or slight extrapolation of parameter values. Experimental sensing, on the other hand, can include either gas-phase species concentrations by techniques such as microprobe mass spectrometry and laser induced fluorescence or morphology of the film over length scales similar to the ones captured by the MC method by scanning probe techniques such as scanning tunneling microscopy.

To further explore the feasibility of such an approach, the results from the DNS were reduced for different step changes in the precursor's mole fraction. The spatiotemporal dynamics obtained from the reduced models was then parameterized as a function of the precursor's bulk mole fraction. More precisely, model reduction was conducted for two perturbations in the precursor's mole fraction (from 2×10^{-4} to 4×10^{-4} and to 6×10^{-4}), and a linear interpolation of the reduced models gave the response for intermediate precursor's mole fraction perturbations. Figure 7 is an illustrative example at 600 K and a strain rate of 100 s^{-1} showing the DNS curve for a step change from 2×10^{-4} to 5×10^{-4} and the trained one resulting from the POD reduced models using five modes. While similar analysis can in principle be performed on the film microroughness, such an increase in the precursor's mole fraction has little effect on the film microroughness. It appears then that small changes in operating conditions may be more easily detectable by gas-phase rather than surface techniques. Similar analysis was performed for a case where extrapolation was necessary (a negative step change from 2×10^{-4} to 1×10^{-4}) giving again satisfactory results.

CONCLUSIONS

We have successfully reduced for the first time the spatiotemporal dynamics of multiscale models coupling continuum fluid phase PDEs and stochastic MC simulations (an SPDE) of the film morphology through proper orthogonal decomposition for a step change in the bulk

concentration of the precursor. Such reduction of complex multiscale systems is an important step for on-line control of film quality. Due to the stochastic nature of a limited number of surface MC snapshots analyzed, satisfactory reduced models for the film can be derived at the expense of higher dimension than that of the gas phase. However, some details of spatial features (e.g., sharpness) are not easily reproduced. Furthermore, it was found that interpolation or extrapolation of parameter values of POD reduced models is feasible. This result is of particular interest for on-line fundamental model based control of microstructure during growth of thin films. Obviously, further advances in *in situ* experimental sensing techniques is highly desirable in order to achieve control of microstructure of miniaturized films and nanoparticles along with application of such reduced models to experimental systems.

ACKNOWLEDGMENTS

Partial support by a National Science Foundation Career Award under Grant CTS-9702615 and useful discussions with Professors I. G. Kevrekidis and T. J. Mountziaris are gratefully acknowledged.

REFERENCES

1. D. G. Vlachos, *AIChE J.* **43**, 3031 (1997).
2. D. G. Vlachos, *Appl. Phys. Lett.* **74**, 2797 (1999).
3. S. T. Rodgers and K. F. Jensen, *J. Appl. Phys.* **83**, 524 (1998).
4. S. T. O'Connell and P. A. Thompson, *Phys. Rev. E* **52**, 5792 (1995).
5. D. G. Vlachos, L. D. Schmidt, and R. Aris, *Phys. Rev. B* **47**, 4896 (1993).
6. P. A. Bui, D. G. Vlachos, and P. R. Westmoreland, *Ind. Eng. Chem. Res.* **36**, 2558 (1997).
7. P.-A. Bui, D. G. Vlachos, and P. R. Westmoreland, *Combust. Flame* **117**, 307 (1999).
8. E. N. Lorenz, MIT, Department of Meteorology Statistical Forecasting Project, Cambridge, MA, 1956.
9. J. L. Lumley, in *Atmospheric Turbulence and Radio Wave Propagation*, edited by A. M. Yaglom and V. I. Tatarski (Moscow: Nauka, 1967), p. 166.
10. L. Sirovich, *J. Comput. Phys.* **96**, 277 (1991).
11. L. Sirovich, *Quart. Appl. Math.* **45**, 561 (1987).
12. L. Sirovich, *Contemp. Math.* **99**, 277 (1989).
13. G. Berkooz, P. Holmes, and J. L. Lumley, *Ann. Rev. Fluid Mech.* **25**, 539 (1993).
14. G. A. Kopp, J. A. Ferre, and F. Giralt, *J. Fluids Eng.* **119**, 289 (1997).
15. L. Sirovich and R. Everson, *Internet. J. Supercomput. Appl.* **6**, 50 (1992).
16. K. Krischer, R. Rico-Martinez, I. G. Kevrekidis, H. H. Rotermund, G. Ertl, and J. L. Hudson, *AIChE J.* **39**, 89 (1993).
17. P. Hasal, J.-L. Montes, H.-C. Boisson, and I. Fort, in *13th International Congress of Chemical and Process Engineering, Prague, Czech Republic, 1998*.
18. S. Y. Shvartsman and I. G. Kevrekidis, *AIChE J.* **44**, 1579 (1998).
19. H. Aling, S. Banerjee, A. K. Bangia, V. Cole, J. Ebert, A. Emami-Naeini, K. F. Jensen, I. G. Kevrekidis, and S. Shvartsman, in *Proceedings of the American Control Conference, Albuquerque, NM, 1997*, p. 2233.
20. H. M. Park and D. H. Cho, *Chem. Eng. Sci.* **51**, 81 (1996).
21. D. A. Goussis and S. H. Lam, in *Symposium (International) on Combustion* The Combustion Institute, Pittsburgh, 1992, Vol. 24, p. 113.
22. U. Maas and S. B. Pope, *Combust. Flame* **88**, 239 (1992).
23. P. Holmes, J. L. Lumley, and G. Berkooz, *Turbulence, Coherent Structures, Dynamical Systems and Symmetry* (Cambridge Univ. Press, New York, 1996).
24. M. A. Katsoulakis and D. G. Vlachos, *Phys. Rev. Lett.* **84**, 1511 (2000).
25. A. E. Deane, I. G. Kevrekidis, G. E. Karniakadis, and S. A. Orszag, *Phys. Fluids A* **3**, 2337 (1991).